KSOE

Journal of Ocean Engineering and Technology 38(2), 43−52, April, 2024
https://doi.org/10.26748/KSOE.2023.038

pISSN 1225-0767
eISSN 2287-6715

Original Research Article

Investigation of Seakeeping Performance of Trawler by the Influence of the Principal Particulars of Ships in the Bering Sea

Thi Thanh Diep Nguyen[1], Hoang Thien Vu[2], Aeri Cho[3] and Hyeon Kyu Yoon[4]

[1]*Researcher, Department of Naval Architecture and Marine Engineering, Changwon National University, Changwon, Korea*
[2]*Graduate Student, Department of Naval Architecture and Marine Engineering, Changwon National University, Changwon, Korea*
[3]*Graduate Student, Department of Smart Environmental Energy Engineering, Changwon National University, Changwon, Korea*
[4]*Professor, Department of Naval Architecture and Marine Engineering, Changwon National University, Changwon, Korea*

KEYWORDS: Trawler, Ship motion responses, Principal dimensions, Seakeeping performance, Sensitive analysis

ABSTRACT: *Investigating ship motion under real conditions is vital for evaluating the seakeeping performance, particularly in the design process stage. This study examined the influence of the principal particulars of a trawler on its seakeeping performance. The wave conditions in the Bering Sea are investigated using available data. The length-to-beam (L/B) and beam-to-draft (B/T) ratios of the ship are changed by 10% for the numerical simulation. The response amplitude operator (RAO) motion, root mean square (RMS) value and sensitivity analysis are calculated to evaluate the influence of the trawler dimensions on ship motions. The peak RAO motion affected the ship motions noticeably because of the resonance at the natural frequency. The L/B and B/T ratios are important geometric parameters of a ship that significantly influence its RMS motion, particularly in the case of roll and pitch. The change in the B/T ratio has a good seakeeping performance based on a comparison of the roll and pitch with the seakeeping criteria. The present results provide insights into the seakeeping performance of ships due to the influence of the principal dimensions in the design stage.*

1. Introduction

The seakeeping performance of a ship needs to be investigated thoroughly to ensure its safety at sea. The ship motions will affect its performance, the activities of the fisherman and the fishing performance of the fishing vessel. In addition, predicting the seakeeping performance of a ship in the sea is one of the most important concerns for naval architects at the design stage. Therefore, seakeeping performance is an important factor influencing the optimization of the ship hull form and its main dimensions. Moreover, considerable improvements in operability, habitability and survivability can be made by changing the main dimensions of the ship. In particular, identifying the principal particulars of the performance of a ship and those related to safety in the early design stage is important.

Many researchers have studied the influence of the hull form parameters of a fishing vessel on its performance. In particular, the impact of the hull form parameters on a ship performance was analyzed, such as the motion response for destroyer hulls (Bales, 1980), ranking of seakeeping performances (van Wijngaarden, 1984; Trincas et al., 2001; Alkan et al., 2003), the response amplitude operators (RAO) motion and root mean square (RMS) motion. On the other hand, the ship parameters also influence the stability and resistance of a ship (Park et al., 2011; Yu et al., 2011; Jeong et al. 2015; Yaakob et al., 2015; Manullang et al., 2017; Kim et al., 2020; Yu et al., 2021). On the other hand, these studies focus on the influence of the principal dimensions on the seakeeping performance. Therefore, research related to this topic was considered in a literature review. Kukner and Aydin (1997) investigated the influence of the ship parameters on the vertical motion of a fishing trawler in head waves. The length-to-beam (L/B) ratio, Froude number and beam-to-draft (L/T) ratio were examined. Moreover, regression analysis was performed to establish the relationship between heave and the ship length. Sayli et al. (2007) investigated the influence of the ship parameters on the heave and pitch. The functional relationships between hull form parameters and seakeeping characteristics of the fishing vessels were identified. Sayli et al. (2010) developed a

Received 17 November 2023, revised 8 January 2024, accepted 12 March 2024
Corresponding author Hyeon Kyu Yoon: +82-55-213-3683, hkyoon@changwon.ac.kr
This paper was presented at 15th International Symposium on Practical Design of Ships and other Floating Structures (Nguyen et al., 2022)

ⓒ 2024, The Korean Society of Ocean Engineers
This is an open access article distributed under the terms of the creative commons attribution non-commercial license (http://creativecommons.org/licenses/by-nc/4.0) which permits unrestricted non-commercial use, distribution, and reproduction in any medium, provided the original work is properly cited.

nonlinear meta-model of heave, pitch and vertical acceleration of a fishing vessel. The seakeeping performance data of the fishing vessel in regular head waves were used. The influence of the hull form parameters on the heave and pitch was obtained. Tello et al. (2011) studied the seakeeping characteristics of a series of fishing vessels to establish the seakeeping criteria for irregular waves. Fishing vessels are considered to operate in sea state 5 and sea state 6 in various Froude numbers and wave directions. The roll and pitch are the most important motion responses of a fishing vessel. Hence, Tello identified the pitch and roll criteria for seakeeping performance in sea state 5 and sea state 6. Cakici and Aydin (2014) identified a relationship between ship parameters and seakeeping characteristics for the YTU Gulet series. The strip method was applied to estimate the ship motion and the statistical short-term was used to analyze the seakeeping performance. The RMS of the heave, pitch and vertical acceleration were investigated in sea state 3 at the head wave.

Sayli et al. (2014) proposed a computer program that analyzed the most influencing parameters on the heave and pitch using a database. Using statistics, the weakest affected parameters were found and removed from the final model. Baree and Afroz (2017) evaluated the seakeeping performance of five series 60 ships regarding the added resistance in various wave directions. The influence of the Froude number, the principal particulars of the ship, wave direction and the seaway were analyzed. Sayli et al. (2016) proposed specifying the relational classification of small vessels based on their form parameters and the seakeeping performance of vertical motion, such as pitch, heave and vertical acceleration. The application was developed in the C# programming language based on the database and the K mean algorithm. Three categories were defined according to the results considering various Froude numbers, loading conditions and the wavelength to the ship length ratio. Manullang et al. (2017) discussed the influence of the ship dimensions and the ship hull shape on the ship motion responses in the following wave, beam wave and head wave. The L/T ratio was changed by 0.2 and 0.4 from the original value. The RMS of the roll and pitch are compared with the criteria reported by Tello et al. (2011).

Against this background, the present study aims to investigate the effect of the ship's principal dimensions of a ship on ship motion response in the Bering Sea. A fishing trawler was chosen to calculate the motion of a ship. First, the sea conditions in the Bering Sea were investigated based on the available data. The wave condition was determined from data obtained from Southeast Bering Sea buoys provided by the National Oceanic and Atmospheric Administration (NOAA). The average significant wave height and average wave period were investigated. Moreover, the average significant wave height and wave period were obtained. The wave conditions were chosen based on the average significant wave height and wave period. The L/B and B/T ratios were changed by 10% to investigate the effects of dimension on the motion responses of a ship. The motion of the fishing trawler was estimated using a numerical method. The RMS of roll and pitch were compared with the fishing vessel criteria suggested by Tello et al. (2011). Finally, the sensitivity of the ship motions due to the influence of the ship dimensions was analyzed. These results can be used to predict the seakeeping performance of fishing vessels and ensure their safety in the design phase.

2. Investigation Wave Condition in the Bering Sea

The trawler fishing vessel in the present study was designed to operate in the Bering Sea. The wave conditions in the Bering Sea were investigated to check the seakeeping performance in real sea conditions. The Bering Sea is one of several biologically productive subarctic seas. Moreover, the Bering Sea biological regime is often described as the richest and most productive. Indeed, the Bering Sea is extremely productive, especially for fish. This study examined the effect of the main ship dimensions on the seakeeping performance in the Bering Sea. The wave conditions in the Bering Sea were investigated to correctly check the seakeeping performance of the fishing vessels that operate in this area. The wave condition was determined using data measured from the Southeast in the Bering Sea buoys provided by NOAA, as shown in Fig. 1 (NOAA, 2022). The statistics for significant wave height and average wave period were investigated. The average significant wave height and wave period were obtained. The wave conditions were collected based on the data in 2022. Fig. 2 presents the significant wave height at the Bering Sea in 2022. A significant wave height is strongly felt in spring and winter due to the effect of storms. On the other hand, the sea is serene in summer and autumn, and the significant wave height changes only slightly. Fig. 3 shows the average wave period in the Bering Sea in 2022. As with the significant wave height, the average wave period is largest in spring and winter. Hence, long and high waves often appear

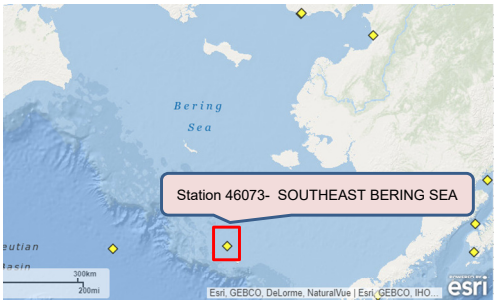

Fig. 1 Buoy position in the Bering Sea

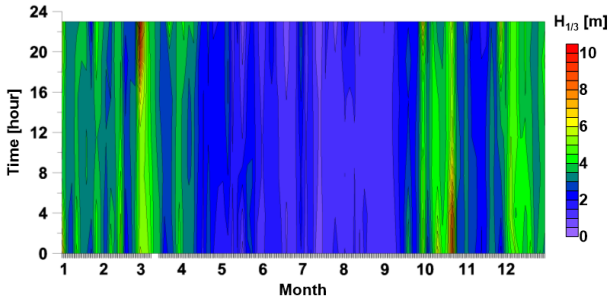

Fig. 2 Significant wave height in 2022

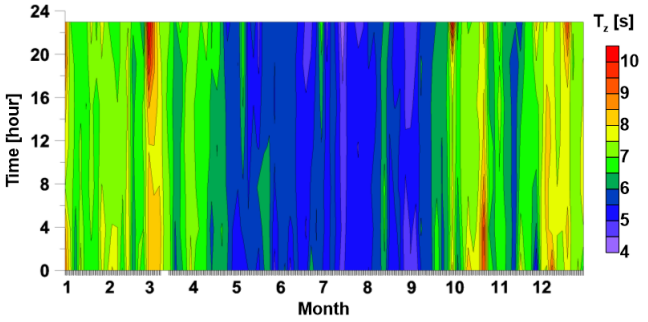

Fig. 3 Wave period in 2022

in the Bering Sea in spring and winter because of the influence of the storms. On the other hand, short and small waves appear in the Bering Sea in summer and autumn. The wave conditions were chosen based on the average significant wave height and wave period. Finally, a sea state with an average significant wave height of 2.44 m and an average wave period of 6.386 s was selected to investigate the seakeeping performance of the trawler fishing vessel.

3. Methodology

3.1 3D Panel Method

In the present study, the six degrees of freedom (6DOF) motion of a ship in regular waves is estimated using the three-dimensional panel method based on the theory of potential. The governing equation becomes the Laplace equation when the fluid is assumed to be inviscid, irrotational and incompressible (Nguyen et al., 2022). The free surface, body boundary and bottom conditions are estimated to calculate the distribution of pressure acting on the ship hull. The three-dimensional Laplace equation of the velocity potential in the fluid domain can be expressed as Eq. (1).

$$\frac{\partial^2\phi}{\partial x^2}+\frac{\partial^2\phi}{\partial y^2}+\frac{\partial^2\phi}{\partial z^2}=0 \tag{1}$$

According to potential theory, the velocity potential need must satisfy Eq. (1) because the velocity potential has the same value at any fluid point. In addition, the boundary condition should be satisfied on the free surface, body and bottom surface. Eq. (2) expresses the classical linear free surface condition of the steady state of the harmonic oscillatory motion of the wave frequency. The bottom boundary condition for the seafloor surface can be represented using Eq. (3). The body boundary condition for the mean wetted hull surface in terms of the diffraction and radiation potential can be expressed as Eqs. (4)–(5). ϕ, ω and d denote the velocity potential, wave frequency and sea depth, respectively.

$$-\omega^2\phi+g\frac{\partial\phi}{\partial z}=0 \quad \text{on} \quad z=0 \tag{2}$$

$$\frac{\partial\phi}{\partial z}=0 \quad \text{on} \quad z=-d \tag{3}$$

$$\frac{\partial\phi}{\partial n}=-\frac{\partial\phi}{\partial n} \quad \text{for diffraction potential} \tag{4}$$

$$\frac{\partial\phi}{\partial n}=-i\omega n_j \quad \text{for radiation potential} \tag{5}$$

The velocity potential is defined by the component of the wave-particle velocity as shown in Eq (6). Eq. (7) expresses the first-order velocity potential. g, ζ, s and θ are the gravity acceleration, wave amplitude, effective water depth and wave phase, respectively.

$$u=\frac{\partial\phi}{\partial x};v=\frac{\partial\phi}{\partial y};w=\frac{\partial\phi}{\partial z} \tag{6}$$

$$\phi^{(1)}=\frac{\zeta g}{\omega}\frac{\cosh ks}{\cosh kd}\sin\theta \tag{7}$$

The total velocity potential is divided into three components: diffraction potential ϕ_D, incident potential ϕ_I and radiation potential ϕ_R. Each component of the velocity potential must satisfy the governing equation in Eq. (1) and the boundary conditions in Eqs. (2)–(5). Eq. (8) expresses the total velocity potential. $\vec{X}=(X,Y,Z)$ is the location point on the body. ϕ_{Rj} and x_j are the potential of radiation waves caused by the ship motion and the ship motion in the j direction, respectively. ω_e is the encounter wave frequency.

$$\phi(\vec{X})e^{-i\omega_e t}=\left[(\phi_I+\phi_D)+\sum_{j=1}^{6}\phi_{Rj}x_j\right]e^{-i\omega_e t} \tag{8}$$

As the velocity potential is obtained, the first-order hydrodynamic distribution of pressure can be estimated using the Bernoulli equation in Eq. (9). ρ is the density of water.

$$p^{(1)}=\rho\left[i\omega_e\phi(\vec{X})+\vec{U}\nabla\phi(\vec{X})\right]e^{-i\omega_e t} \tag{9}$$

The first-order hydrodynamic forces on a ship can be determined by integrating the water pressure on the wetted surface using the pressure distribution. The first-order hydrodynamic forces on the body can be calculated using Eq. (9). Eq. (10) describes the first-order wave force by combining Eqs. (8) and (9). n_j and S are the unit normal vector and mean wetted surface of the ship hull, respectively. The total first-order hydrodynamic force can be written as Eq. (11). F_{Ij}, F_{Dj} and F_{Rjk} are the Froude-Krylov force, diffraction force and radiation force, respectively. These hydrodynamic forces can be calculated using Eqs. (11)–(14).

$$F_j e^{-i\omega_e t}=-\int_{S_0}p^{(1)}n_j dS=-\rho\left[(i\omega_e+\vec{U}.\nabla)\phi(\vec{X})\right]n_j dS \tag{10}$$

$$F_j=\left[(F_{Ij}+F_{Dj})+\sum_{k=1}^{6}F_{Rjk}x_k\right],j=1,\cdots,6 \tag{11}$$

$$F_{Ij}=-\rho\int_{S_0}\left[(i\omega_e+\vec{U}.\nabla)\phi_I(\vec{X})\right]n_j dS \tag{12}$$

$$F_{Dj} = -\rho \int_{S_0} \left[(i\omega_e + \vec{U}.\nabla)\phi_D(\vec{X}) \right] n_j dS \quad (13)$$

$$F_{Rjk} = -\rho \int_{S_0} \left[(i\omega_e + \vec{U}.\nabla)\phi_{Rk}(\vec{X}) \right] n_j dS \quad (14)$$

3.2 RMS Motion

The seakeeping performance of the ship is checked by calculating the RMS motion based on the irregular wave conditions and the RAO motion of the ship. The energy spectrum is estimated using Eqs. (15)–(17). z denotes heave. ϕ and θ denote roll and pitch, respectively. k is the wave number. The RMS motion value is determined as the square root of the variances. The variances and the RMS value of motion can be estimated using Eqs. (18)–(21), respectively. In order to estimate the wave spectrum $S(\omega)$, the ITTC spectrum was calculated using Eq. (22) (ITTC, 2014). $H_{1/3}$ and T_1 are the significant wave height and average wave period, respectively. In the case of the following and quartering waves, the wave frequency is considered to replace the encounter frequency to calculate the RMS motion to avoid the singularity in the encounter wave spectrum (Lewis, 1988).

$$S_z(\omega_e)d\omega_e = \left(\frac{z}{\zeta}\right)^2 S_\zeta(\omega_e)d\omega_e = RAO_z^2 S_\zeta(\omega_e)d\omega_e \quad (15)$$

$$S_\phi(\omega_e)d\omega_e = \left(\frac{\phi}{k\zeta}\right)^2 k^2 S_\zeta(\omega_e)d\omega_e = RAO_\phi^2 S_\alpha(\omega_e)d\omega_e \quad (16)$$

$$S_\theta(\omega_e)d\omega_e = \left(\frac{\theta}{k\zeta}\right)^2 k^2 S_\zeta(\omega_e)d\omega_e = RAO_\theta^2 S_\alpha(\omega_e)d\omega_e \quad (17)$$

where, $S_\alpha(\omega_e) = \frac{\omega^2}{g} S_\zeta(\omega_e) = k^2 S_\zeta(\omega_e)$.

$$m_{0_z} = \int_0^\infty S_z(\omega_e)d\omega_e \quad (18)$$

$$m_{0_\phi} = \int_0^\infty S_\phi(\omega_e)d\omega_e \quad (19)$$

$$m_{0_\theta} = \int_0^\infty S_\theta(\omega_e)d\omega_e \quad (20)$$

$$\sigma_z = \sqrt{m_{0_z}} \;;\; \sigma_\phi = \sqrt{m_{0_\phi}} \;;\; \sigma_\theta = \sqrt{m_{0_\theta}} \quad (21)$$

$$S_\omega = \frac{A}{\omega^5} e^{-\frac{B}{\omega^4}} \quad (22)$$

$$A = 173(H_{1/3})^2/T_1^4 \;;\quad B = 691/T_1^4 \quad (23)$$

3.3 Sensitivity Analysis

In sensitivity analysis, a sensitivity index measures how sensitive the output of a model is to changes in its input parameters or variables. It quantifies the degree to which variations in the inputs affect the output. A higher sensitivity index indicates that a small change in the input parameter has a significant impact on the output, while a lower sensitivity index suggests that the output is less sensitive to changes in that particular input. The sensitivity index for RMS motion S_{ijk} is estimated using Eq. (24). H^* denotes the origin principal dimension of the ship. H represents the deviated value of the principal dimensions of a ship. R^* denotes the value of the corresponding RMS motion value obtained from the original ship using H^*. R represents the corresponding RMS motion values obtained from the modified ship using H. S_{ijk} is the sensitivity index for the i^{th} RMS motion for the $k\%$ change in the j^{th} principal dimension. The influence of principal dimensions on the seakeeping performance, such as the RMS motion, is considered.

$$S_{ijk}^* = \frac{|R - R^*|/R^*}{|H - H^*|/H^*} \quad (24)$$

4. Target Ship and Test Condition

In this study, a fishing trawler is selected to perform assess the seakeeping performance in the Bering Sea. The principal particulars of the fishing trawler in the case of the original are summarized in Table 1. Fig. 4 shows the modeling of the fishing trawler used in the present research. The *L/B* and *B/T* ratios are changed by 10% to investigate the effects of dimensions on the ship's motion response. In the case of a change in the *L/B* ratio, *L* was changed by ± 10% and *B* was kept constant and *B* was changed by ± 10 % and *T* was kept constant in the case of *B/T*. In order to estimate the RMS motion, the numerical simulation of the motion RAO of the fishing trawler is performed at a ship speed of 6 knots. The simulation is conducted to examine the effect of regular waves on the fishing trawler in various wave directions and provide the input data of the RAO motion responses for calculating irregular wave motion responses. The range of wave directions is from 0 degrees to 180 degrees at 30 degrees intervals. The wave frequency ranges from 0.3 rad/s to 3.0 rad/s in 0.1 rad/s intervals. The wave directions are defined, as shown in Fig. 5. In the case of irregular waves, a sea state with an average significant wave height of 2.44 m and an average wave period of 6.386 s were selected to investigate the seakeeping performance of the trawler fishing vessel. Furthermore, according to the ITTC recommendation for numerical estimation of roll damping, roll damping was significantly affected by the viscous effect. In this study, the additional roll damping for the fishing vessel was divided into 5 components: wave making, hull lift, frictional, eddy making and skeg component (ITTC, 2011).

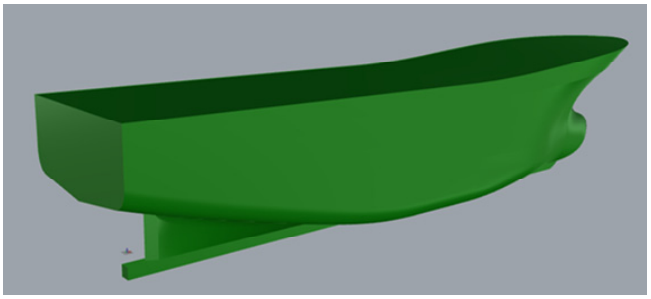

Fig. 4 Trawler fishing vessel

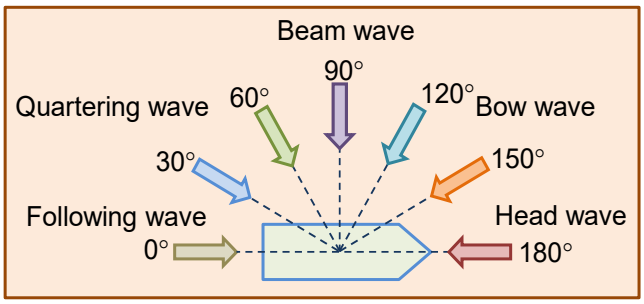

Fig. 5 Definition of the wave direction

Table 1 Principal dimensions

Item	Unit
Length between perpendiculars, L (m)	32.450
Beam, B (m)	9.000
Displacement, △ (t)	587.000
Draft, T (m)	3.000
Speed, U (m/s)	3.086
Roll radius of gyration, k_{xx} (m)	0.400 B
Pitch radius of gyration, k_{yy} (m)	0.250 L
Yaw radius of gyration, k_{zz} (m)	0.250 L
Vertical center of gravity, VCG (m)	3.590

5. Result and Discussion

5.1 RAO Motion

A numerical simulation of the motion RAO of the fishing trawler is carried out to estimate the RMS motion. The effect of the regular waves on the fishing trawler in various wave directions is investigated. The L/B and B/T ratios are changed by 10% to investigate the effect of dimension on the ship's motion response. The natural frequency of heave, roll and pitch are calculated due to the influence of a change in the main dimensions of the ship. The natural frequencies of heave, roll and pitch can be determined using Eqs. (25)–(27). m, m_a and A_W denote the mass of the ship, added mass and water plane area, respectively. GM_T and GM_L are the transverse and longitudinal metacentric heights of the ship, respectively. I_{xx} and I_{yy} are the roll and pitch moment of inertia of the ship, respectively. J_{xx} and J_{yy} are the added inertia moment in roll and pitch, respectively. Table 2 lists the natural frequencies due to the influence of the ship dimensions.

$$\omega_{n_z} = \sqrt{\frac{\rho g A_W}{m+m_a}} \tag{25}$$

$$\omega_{n_\phi} = \sqrt{\frac{mgGM_T}{I_{xx}+J_{xx}}} \tag{26}$$

$$\omega_{n_\theta} = \sqrt{\frac{mgGM_L}{I_{yy}+J_{yy}}} \tag{27}$$

Table 2 Natural frequency

Item	Heave (rad/s)	Roll (rad/s)	Pitch (rad/s)
Original	1.486	0.703	1.547
L/B + 10%	1.488	0.706	1.556
L/B − 10%	1.487	0.704	1.536
B/T + 10%	1.489	0.840	1.571
B/T − 10%	1.489	0.493	1.571

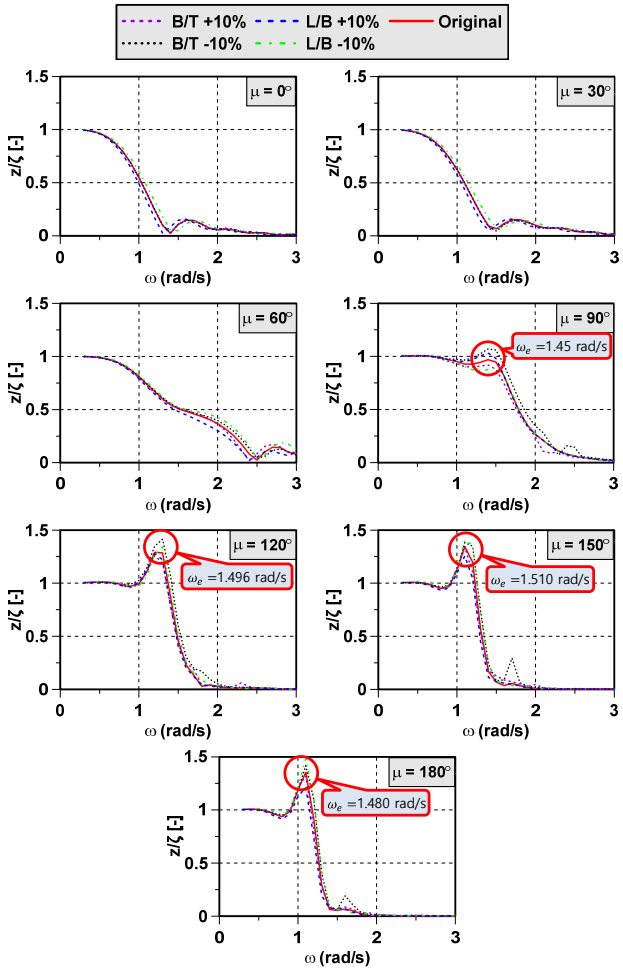

Fig. 6 Heave RAO

Fig. 6 compares the heave RAO according to the change in L/B, B/T ratios and wave directions. The greatest heave RAO of the ship occurs when the wave direction approaches 180 degrees. As the wave frequency increases, the heave RAO tends to decrease. In short waves, however, the heave decreases to zero, especially when the wavelength is short compared to the ship length. The heave RAO tends to be 1 in the long waves because the heave follows the wave elevation. The heave RAO varies slightly depending on the ship dimensions. In general, the heave RAO is the largest when the B/T ratio was reduced by 10% when the wave direction approaches 90 degrees. On the other hand, the heave RAO is the largest when the L/B ratio is reduced by 10% and the wave direction approaches 180 degrees. Hence, the heave RAO does not depend much on the ship dimension. The numerical

results showed that the heave RAO is the largest when the encounter frequency is close to the heave natural frequency. The heave RAO depends on the water plane area and the ship displacement. The ship displacement and water plane area increased when the *L*/*B* and *B*/*T* ratios were increased by 10%. The displacement and waterplane area of a ship are proportional to each other; therefore, the heave natural frequency does not change when the principal dimensions are changed. Table 2 lists the natural frequency of heave according to the *L*/*B* and *B*/*T* ratio.

Fig. 7 shows the roll RAO at various *L*/*B* and *B*/*T* ratios and wave directions. The numerical results showed that the roll RAO becomes dominant when the wave direction is close to 90 degrees and decreases as the wave direction approached 0 degrees and 180 degrees. The roll RAO with different *B*/*T* ratios changes dramatically in various wave directions because of the effect of the breadth of the ship. The roll RAO decreases as the wave frequency increases. The peak roll RAO occurs at an encounter frequency close to the natural frequency of the roll. The numerical results of the roll RAO in the beam wave showed that the peak roll RAO according to the *L*/*B* ratio and the ship origin occurs at encounter frequency of 0.7 rad/s. This value is approximately the roll natural frequency according to the *L*/*B* ratio and the original ship. The peak roll RAO when the *B*/*T* ratio is reduced by 10% occur at the encounter frequency of 0.9 rad/s, which is close to the roll natural frequency of *B*/*T* ratio reduced by 10%. The peak roll RAO when the *B*/*T* ratio is increased by 10% occurs at an encounter frequency of 0.5 rad/s, which is approximately the roll natural frequency of the *B*/*T* ratio increased by 10%.

Fig. 8 presents the numerical results of the pitch RAO of the various *L*/*B* and *B*/*T* ratios and wave directions. The largest pitch RAO of the ship occurs when the wave direction approaches 0 degrees due to the effect of the forward speed. The pitch RAO tended to decrease significantly as the wave frequency increases. Moreover, the pitch response is combined with the heave. Therefore, the motion responses of heave and pitch are the same phenomenon. The pitch RAO is the largest for the *L*/*B* ratio reduced by 10%. From the numerical results, the peak pitch RAO occurs at a wave frequency near the pitch natural frequency. The numerical results of the pitch RAO in the head wave showed that the peak pitch RAO in the original ship occurs at an encounter frequency of 1.5 rad/s. This is approximately the pitch natural pitch frequency of the original ship. The peak pitch RAO when the *L*/*B* ratio was increased by 10% occurs at an encounter frequency of 1.566 rad/s and a wave direction of 120 degrees. The peak pitch RAO when the *L*/*B* ratio is decreased by 10% occurs at an encounter frequency of 1.510 rad/s and a wave direction of 150 degrees. The

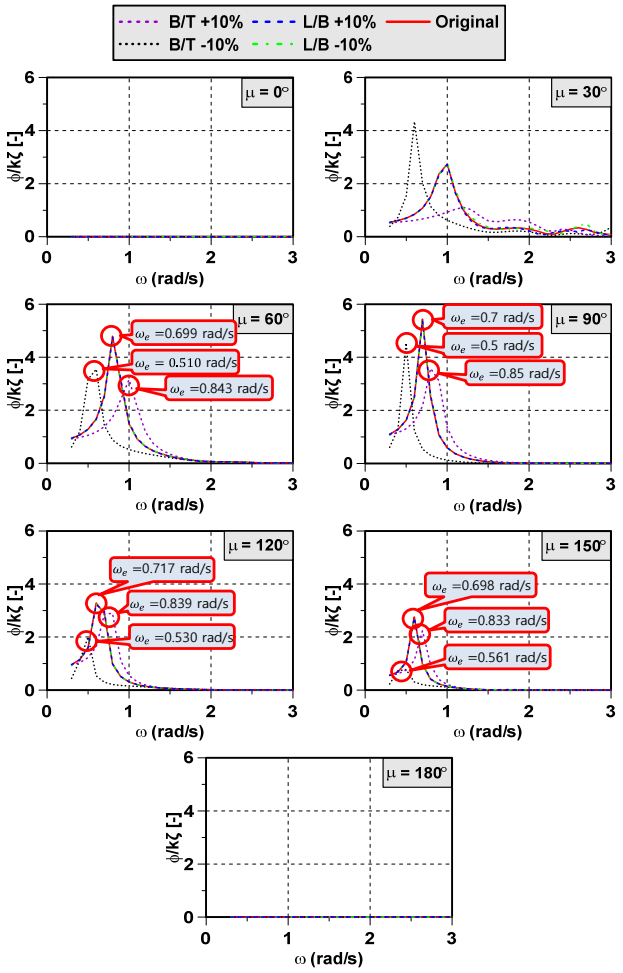

Fig. 7 Roll RAO

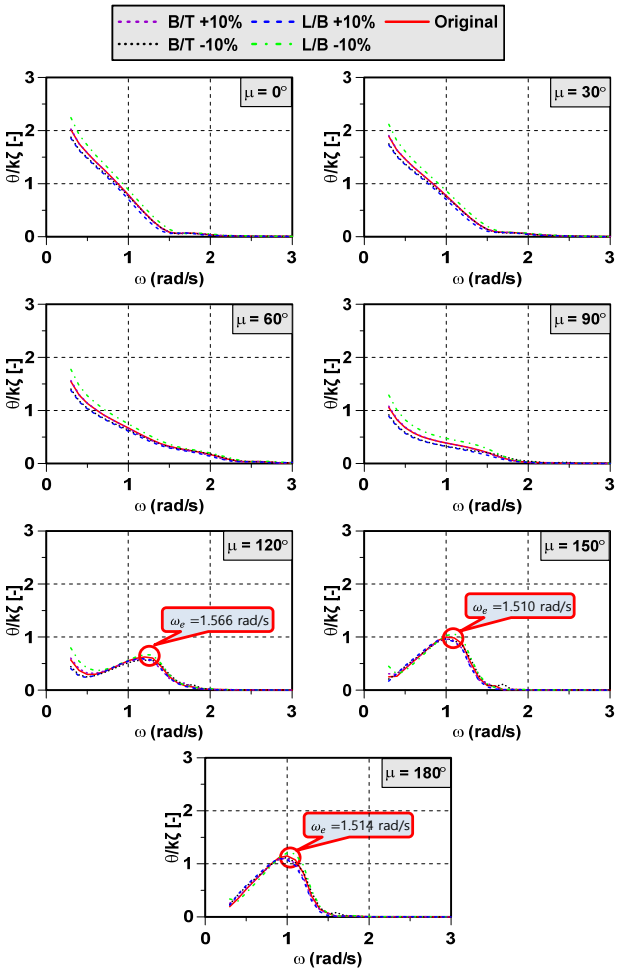

Fig. 8 Pitch RAO

peak pitch RAO when the *B/T* ratio is increased by 10% occurs at an encounter frequency of 1.514 rad/s at a wave direction of 180 degrees. Generally, the peak heave, roll and pitch occur at an encounter frequency close to the natural frequency. Table 2 lists the natural frequency of the heave, roll and pitch due to a change in the ship dimensions.

The ship motion responses are affected noticeably in the peak values due to a change in the *L/B* and *B/T* ratios because of resonance at the natural frequency. The varied ship dimensions affect the inertia moment, displacement and roll damping coefficient directly. The heave tends to increase when the displacement increases. A longer ship may have a longer waterline, which can affect the buoyancy distribution and the response to wave-induced heave. Longer ships tend to experience a reduced pitch. The longer waterline provides more resistance to pitch, and the ship is less sensitive to changes in trim caused by pitching. The increased inertia caused by the longer length contributes to a smoother response to wave-induced pitch motions. Furthermore, the roll is influenced the most by the beam of the ship. Hence, the roll period can determine the comfort of those operating on board.

5.2 RMS Motion

In the case of irregular waves, a sea state is chosen to estimate the wave spectrum in the Bering Sea based on the results of the investigated wave conditions. The average significant wave height and wave period were 2.44 m and 6.386 s, respectively. The ITTC spectrum recommended by the International Towing Tank Conference was used to estimate the wave spectrum.

Fig. 9 compares the RMS heave in the original ship to the RMS heave in the ship with changed ratios of *L/B* and *B/T*. The heave is the strongest in the bow wave, head wave and beam wave. The RMS heave changes slightly as the principal dimensions of the ship changed. In the case of increased and decreased *L/B* ratio, the RMS heave varied by −4.841% and 4.312% in the head wave, respectively, compared to the original case. In the case of increased and decreased *B/T* ratio, the RMS heave varied by −0.270% and 2.561% in the head wave, respectively, compared to the original case.

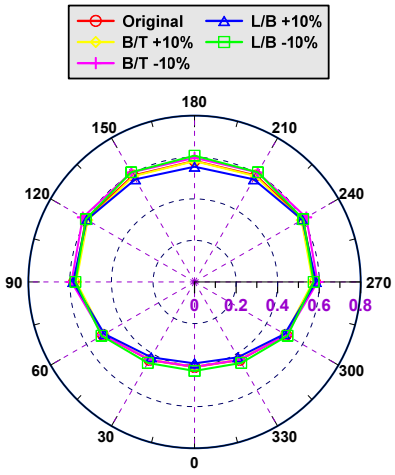

Fig. 9 RMS heave (m)

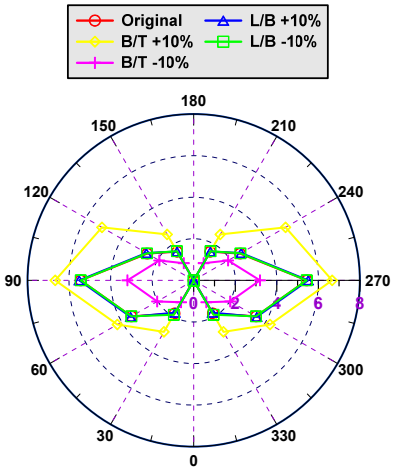

Fig. 10 RMS roll (deg.)

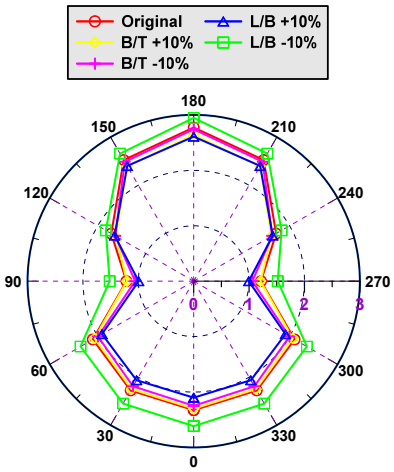

Fig. 11 RMS pitch (deg.)

Fig. 10 compares the RMS roll in the original ship to the RMS roll in the ship according to the *L/B* and *B/T* ratios. The roll changes noticeably in various wave directions. The strongest roll is observed with a wave direction of 90 degrees. The breadth of a ship strongly influences the motion responses, particularly the roll. Based on the RMS roll, the effect of the ship length is not significant. In the case of increased and decreased *L/B* ratio, the RMS roll varied by 1.285% and −0.023% in the beam wave compared to the original case. In the case of increased and decreased *B/T* ratio, the RMS roll varied by 22.514% and −41.347% in the beam wave, respectively, compared to the original case.

The comparison of the RMS pitch in the original ship to the RMS pitch in the ship according to the *L/B* and *B/T* ratios is shown in Fig. 11. The pitch changes strongly in various wave directions. The strongest pitch motion is observed at the head wave. The smallest pitch occurs at the beam wave. On the other hand, the pitch at a wave direction of 90 degrees does not become zero due to the effect of the forward speed. The pitch motion increases dramatically as the wave direction ranges nearly to quartering waves. The principal particulars of the ship strongly affect the pitch motion. Based on the RMS pitch,

Table 3 Verification of the seakeeping criteria in sea state 5 (Satisfied: O; Unsatisfied: X)

Item	Roll RMS (deg.)			Pitch RMS (deg.)		
	Max.	Criteria	Satisfied	Max.	Criteria	Satisfied
Original	6.572	6	X	2.773	3	O
L/*B* + 10%	6.612		X	2.609		O
	6.530		X	2.945		O
	5.938		O	2.642		O
	2.932		O	2.741		O

the effect of the ship's length is larger than the ship's breadth, particularly when the *L*/*B* ratio is decreased by 10%. In the case of increased and decreased *L*/*B* ratio, the RMS pitch varied by −5.910% and 6.201% in the head wave, respectively, compared to the original case. In the case of increased and decreased *B*/*T* ratio, the RMS pitch varied by −4.724% and −1.150% in the head wave, respectively, compared to the original case.

The seakeeping performance is checked by comparing the maximum roll and RMS pitch with the seakeeping criteria suggested by Tello et al. (2011), as listed in Table 3. The pitch motion can meet the seakeeping criteria in the origin ship and the ship with changed *L*/*B* and *B*/*T* ratios. On the other hand, the RMS roll was slightly greater than the seakeeping criteria, except in the case of a change in *B*/*T* ratio.

5.3 Sensitivity Analysis

Sensitivity analysis of the *L*/*B* and *B*/*T* ratios is done by deviating each *L*/*B* and *B*/*T* ratio by 10%. Figs. 12−14 show the effects of the *L*/*B* and *B*/*T* ratios on the RMS heave, roll and pitch, respectively. The sensitivity of the RMS heave is the highest in the head wave and the following wave. Moreover, the *L*/*B* ratio has the greatest influence on the RMS heave. Similar to the same trend of the RMS heave, the *L*/*B* ratio also has the greatest impact on the RMS pitch. The reason for such relationships is the coupling of the heave and pitch motions. The sensitivity of the RMS pitch increases noticeably with the following wave and stern waves. In contrast to the sensitivity of the heave and RMS pitch, the RMS roll sensitivity becomes zero in the following wave and the heave wave because of the direction of the incident wave. The RMS roll sensitivity is strongly affected by the *B*/*T*, ratio, especially at a wave direction of 120 degrees. The *L*/*B* ratio has a negligible influence on the RMS roll sensitivity.

The *L*/*B* and *B*/*T* ratios are important geometric parameters of a ship that significantly influence its RMS motion. The *L*/*B* and *B*/*T* ratios influence the ship motions through their effects on stability, buoyancy distribution, displacement and the response of the ship to wave-induced forces. The sensitivity index of the RMS heave changes slightly in various wave directions. In other words, the sensitivity of RMS heave is negligible under the influence of the *L*/*B* and *B*/*T* ratio. Nevertheless, the sensitivity index of the RMS roll varies significantly in various wave directions because of the influence of the B/T ratio and the roll is influenced the most by the breadth of the ship. In the

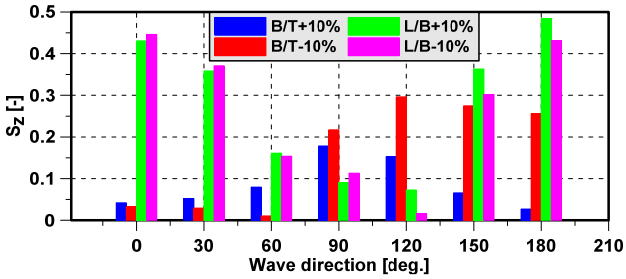

Fig. 12 Sensitivity index of RMS heave

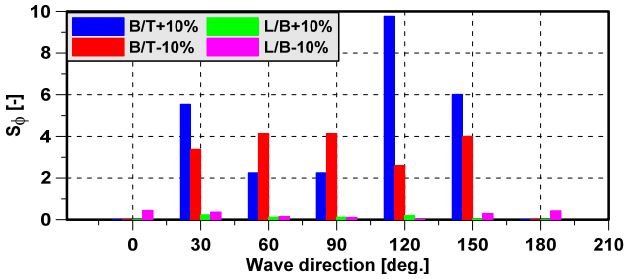

Fig. 13 Sensitivity index of RMS roll

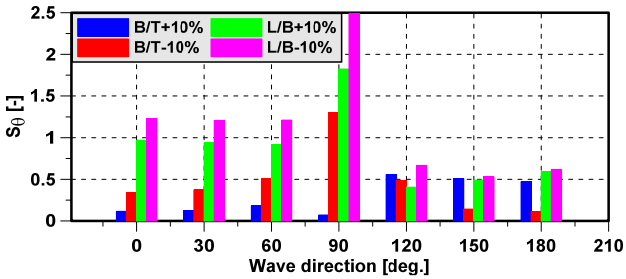

Fig. 14 Sensitivity index of RMS pitch

case of pitch, the sensitivity index of the RMS pitch changes drastically due to the influence of the *L*/*B* ratio.

6. Conclusion

This paper reported the effects of the principal dimensions of a ship on a trawler fishing vessel in the Bering Sea. The final remarks are as follows:

First, the sea condition in the Bering Sea was investigated based on the available data. The statistics of significant wave height and average wave period were analyzed. A sea state was then chosen using the average value of the significant wave height and wave period.

Second, the *L*/*B* and *B*/*T* ratios were changed by 10% to determine the effect of the dimension on the motion responses of a ship. As shown in the RAO and RMS motion results, the *L*/*B* ratio affected the heave and pitch. In contrast, the roll was influenced substantially by the *B*/*T* ratio. Moreover, the influence of the *L*/*B* and *B*/*T* ratios on the RMS motion was also investigated. The maximum RMS roll and pitch were compared with the seakeeping criteria suggested by Tello et al. (2011).

Third, the sensitivity index of the *L*/*B* and *B*/*T* ratios on the RMS

heave, roll and pitch was analyzed. The sensitivity of the RMS heave was highest in the head wave and the following wave. The heave and the pitch were coupled. Therefore, the sensitivity trends of the heave and the pitch are similar and the *L*/*B* ratio has the largest impact on the RMS heave and pitch. In contrast to the sensitivity of the RMS heave and RMS, the sensitivity of the RMS roll becomes zero in the following wave and heave wave because of the direction of the incident wave. The sensitivity of the RMS roll is strongly affected by the *B/T* ratio, especially at a wave direction of 120 degrees. The *L*/*B* ratio has a negligible influence on the sensitivity of the RMS roll.

Finally, the change in *B/T* ratio has a good seakeeping performance based on a comparison of the roll and pitch with the seakeeping criteria. On the other hand, the increased beam can cause ship stability problems due to a change in the righting arm (GZ) curve because the inflection point of the GZ curve occurs at a small inclination angle. The reduced beam shortens the natural period of a ship. Its acceleration and comfort are affected. In addition, the *B/T* ratio influences the wave-making resistance. Generally, lower *B/T* ratios are associated with lower wave resistance, leading to better propulsion efficiency. Nevertheless, extremely low *B/T* ratios may increase the susceptibility to parametric rolling. On the other hand, the change in *L*/*B* has less seakeeping performance, particularly in roll based on a comparison of roll seakeeping criteria. A higher *L*/*B* ratio generally contributes to better stability in waves. Longer ships tend to have smoother motions and are less prone to rolling, which is particularly important for passenger comfort and safety. Longer ships experience less wave resistance, leading to improved fuel efficiency, but extremely long and slender ships may face challenges related to structural strength. Although these ratios provide insights into the seakeeping performance of a ship, they are just one set of parameters that naval architects should consider. The actual impact of these ratios depends on various factors, including the specific design, the purpose of the ship, operational conditions, and intended trade routes.

Conflict of Interest

Hyeon Kyu Yoon serves as a journal publication committee member of the Journal of Ocean Engineering and Technology, but he had no role in the decision to publish this article. The authors have no potential conflict of interest relevant to this article.

Funding

This work was supported by the Korea Institute for Advancement of Technology (KIAT) grant funded by the Korean Government (MOTIE) (P0017006, The Competency Development Program for Industry Specialist).

References

Alkan, A. D., Ozmen, G., & Gammon, M. A. (2003). Parametric relation of seakeeping. In *9th International Symposium on Technics and Technology in Fishing Vessels.*

Bales, N. K. (1980). Optimizing the seakeeping performance of destroyer type hulls. In *13th Symposium on Naval Hydrodynamics.*

Baree, M. S., & Afroz, L. (2017). Seakeeping performance of series 60 ships. *Procedia Engineering, 194*, 189−196. https://doi.org/10.1016/j.proeng.2017.08.134

Cakici, F., & Aydin, M. (2014). Effects of hull form parameters on Seakeeping for YTU gullet series with cruiser stern. *International Journal of Naval Architecture and Ocean Engineering*, *6*(3), 700−714. https://doi.org/10.2478/IJNAOE-2013-0206

ITTC. (2011). *Recommended procedures and guidelines: Numerical estimation of roll damping* (7.5-02-07-04.5). https://www.ittc.info/media/8151/75-02-07-045.pdf

ITTC. (2014). *Recommended procedures and guidelines: Seakeeping experiments* (7.5-02-07-02.1). https://www.ittc.info/media/8101/75-02-07-021.pdf

Jeong, U. C., Kim, H. S., Kwon, S. Y., & Choi, J. H. (2015). Study of hull form development of 5-ton-class catamaran-type coastal fishing boat for welfare accommodation of fishing crew. *Journal of Ocean Engineering and Technology*, *29*(6) 405−410. https://doi.org/10.5574/KSOE.2015.29.6.405

Kim, M. S., Hwang, B. K., & Chang, H.Y. (2020). Analysis of efficiency of fishing operation by the change in the size of coastal composite fishing boat. *Journal of the Korean Society of Fisheries and Ocean Technology*, 56(2), 126−137. https://doi.org/10.3796/ KSFOT.2020.56.2.126

Kukner, A., & Aydin, M. (1997). Influence of design parameters on vertical motion of trawler hull forms in head seas. *Journal of Marine Technology and SNAME News*, 34(3), 181−196. https://doi.org/10.5957/mt1.1997.34.3.181

Lewis, E. V. (Ed.). (1988). *Principal of Naval Architecture: vol. III - Motion in Waves and Controllability*. The Society of Naval Architects and Marine Engineers.

Manullang, S., Fadillah, A., & Irvana, R. (2017). Analysis of stability, resistance and seakeeping accord to dimension and form of fishing vessel 30 GT. *Marine Technology for Sustainable Development*, 68−75.

National Oceanic and Atmospheric Administration (NOAA). (2022). *Station 46073 (LLNR 1199) − Southeast Bering Sea - 205 NM WNW of Dutch Harbor, AK.* Historical data - Standard meteorological data. https://www.ndbc.noaa.gov/station_history.php?station=46073

Nguyen, T. T. D., Nguyen, V. M., & Yoon, H. K. (2022). Experimental and numerical simulation on dynamics of a moored semi-submersible in various wave directions. *Science Progress*, *104*(4). https://doi.org/10.1177/0036850422109600

Park, R. S., Kim, S. G., & Lee, J. B. (2011). Study on motion response characteristics for large inclined state of small fishing vessel in

beam sea condition, *Journal of Ocean Engineering and Technology*, *25*(6). 17−22. https://doi.org/10.5574/KSOE.2011.25.6.017

Sayli, A., Alkan, A. D., & Aydin, M. (2016). Determination of relational classification among hull form parameters and ship motions performance for a set of small vessels. *Brodogradnja*, *67*(4), 1−15. https://doi.org/10.21278 /brod67401

Sayli, A., Alkan, A. D., & Ganiler, O. (2010). Nonlinear meta-models for conceptual seakeeping design of fishing vessels. *Ocean Engineering*, *37*(8−9), 730−741. https://doi.org/10.1016/j.oceaneng.2010.02.005

Sayli, A., Alkan, A. D., Nabergoj, R., & Uysal, A. O. (2007). Seakeeping assessment of fishing vessels in conceptual design stage. *Ocean Engineering*, *34*(5−6), 724−738. https://doi.org/10.1016/j.oceaneng.2006.05.003

Sayli, A., Alkan, A. D., & Uysal, A. O. (2014). Automatic elimination of ship design parameters based on data analysis for seakeeping performance. *Brodogradnja/Shipbilding*, *65*(4), 1−19.

Tello, M., Silva, S. A., & Soares, C. G. (2011). Seakeeping performance of fishing vessels in irregular wave. *Ocean Engineering*, *38*, 763−773, https://doi.org/10.1016/j.oceaneng.2010.12.020

Trincas, G., Nabergoj, R., & Messina, G. (2001). Inverse problem solution to identify optimal hull forms of fishing vessels for efficient operation. In *8th International Symposium on Technics and Technology in Fishing Vessels.*

van Wijngaarden, A. M. (1984). The optimum form of a small hull for the North Sea area. *International Shipbuilding Progress*, *31*(359), 181−187. https://doi.org/10.3233/ISP-1984-3135902

Yaakob, O., Hashim, F. E., Jalal, M. R., & Mustapa, M. A. (2015). Stability, seakeeping and safety assessment of small fishing boats operating in southern coast of Peninsular Malaysia. *Journal of Sustainability Science and Management*, *10*(1), 50−56.

Yu, J. W., Lee, M. K., Kim, Y. I., Suh, S. B., & Lee, I. (2021). An optimization study on the hull form and stern appendage for improving resistance performance of a coastal fishing vessel. *Applied Sciences*, *11*(6124), 6124. https://doi.org/10.3390/app11136124

Yu, J. W., Lee, Y. G., Park, A. S., Ha, Y. J., Park, C. K., & Choi, Y. C. (2011). A study on the resistance performance of Korean high speed small coastal fishing boat. *Journal of the Society of Naval Architects of Korea*, *48*(2), 158−164. https://doi.org/10.3744/SNAK.2011.48.2.158

Author ORCIDs

Author name	ORCID
Nguyen, Thi Thanh Diep	0000-0003-3521-6680
Vu, Hoang Thien	0000-0001-8147-0597
Cho, Aeri	0009-0006-0014-1729
Yoon, Hyeon Kyu	0000-0001-6639-0927